ZERO BIAS H_∞ CONTROL OF ACTIVE MAGNETIC BEARINGS FOR ENERGY STORAGE FLYWHEEL SYSTEMS

Toshiyuki NAKAMURA, Mitsuo HIRATA, and Kenzo NONAMI
Department of Electronics and Mechanical Engineering, Chiba University
1-33 Yayoi-cho, Inage-ku, Chiba 263-8522
mitsuo_hirata@faculty.chiba-u.jp, nonami@faculty.chiba-u.jp

ABSTRACT

For energy storage flywheel systems, the reduction of energy loss of AMBs is a very important subject. Thus, the control method based on bias current is not appropriate for these systems because it consumes energy even if the rotor is controlled at the equilibrium point. In this paper, we propose a simple and effective method which does not use bias current based on a simple linearization and the H_∞ control. The H_∞ method can design a robust controller systematically. The effectiveness of the proposed method is shown by simulation and experiment.

INTRODUCTION

Active magnetic bearings (AMBs) can support a rotor without contact by electromagnetic force. Therefore these systems have lots of advantages such as no wear and friction, noiseless, and no lubrication, and it can achieve ultra-high-speed rotation. Recently, the AMBs have been applied to various fields: turbo-molecular pumps, flywheel energy storage systems, and artificial heart systems. Especially flywheel energy storage systems, which store electric energy as kinetic energy by high speed rotation of flywheel, have been progressed remarkably. Until now, slide bearings and ball bearings, which are filled with lubrication at supporting points, have been applied to the flywheel energy storage systems, however the bearings have limitation of the maximum rotation speed because of the friction caused by lubrication. Hence the AMBs are expected to be an innovative solution of the conventional bearings for flywheel systems.

Since the AMBs are nonlinear and unstable systems, the feedback control is necessary to levitate a rotor. In general, the linear control theory is commonly used and the linearized model of the AMBs is obtained by supplying a bias current to a pair of electromagnets facing each other. However, this method always requires the bias current even if the rotor can be controlled at the equilibrium point, and it makes power consumption be large. Furthermore, the bias current causes an eddy current loss. Especially for the energy flywheel system, the reduction of the energy loss of the AMB is a very important subject. In [2], [3], nonlinear control methods have been proposed, however, the design procedure is not necessarily simple, and it is difficult to design a controller considering the trade-off between the control performance and the robust stability to the unmodeled dynamics.

In this paper, we propose a simple and effective method which does not use the bias current based on a simple linearization and the H_∞ control. We focus on the fact that the flywheel system supported by the AMBs becomes a linear system if the forces generated by electromagnets are regarded as the control input, and the H_∞ controller, where the control input is assumed to be the electromagnetic forces, is designed to have a good disturbance rejection and robustness to a plant uncertainty. The coil currents are calculated by nonlinear equations in real-time to generate the forces corresponded to the output of the H_∞ controller. The effectiveness of the proposed method is shown by simulation and experiment. The reduction of the energy loss is also evaluated comparing to the conventional method using bias current.

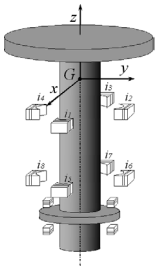

FIGURE 1: A five-degree-of-freedom AMB system equipped with a flywheel for energy storage

MODELING

Fig. 1 shows the schematic diagram of a five-degree-of-freedom AMB system with a flywheel. As for the axial direction, the rotor is already controlled by a conventional PID controller. For simplicity, the gyroscopic effect is not considered, and it is assumed that the interaction between X-Z and Y-Z planes can be neglected. Fig. 2 shows the schematic diagram of X-Z plane of the AMB with flywheel, and the physical parameters are shown in Table 1. From Fig. 2, we could obtain the equation of motions of parallel mode and rotational mode as follows:

$$M\ddot{x} = f_u + f_l, \tag{1}$$

$$I_r\ddot{\theta}_x = -f_u l_u - f_l l_l, \tag{2}$$

where x is the displacement at the centre of gravity, θ_x is the angle of the rotation around the Y axis, and f_u and f_l are the attraction forces generated by the upper and the lower AMB respectively. Let the output y_u and y_l of the system be

$$y_u = x - l_1\theta_x \; C \qquad y_l = x - l_2\theta_x. \tag{3}$$

TABLE 1: Parameters

Symbol		Value
M_f:	Mass of rotor	13.672 [kg]
I_{fr}:	Moment of inertia about x and y axis	1.73×10^{-1} [kgm^2]
k_{fu}:	Force coefficient	4.47×10^{-6} [Nm^2/A^2]
k_{fl}:	(upper & lower)	3.10×10^{-6} [Nm^2/A^2]
X_0, Y_0:	Nominal air gap	0.25×10^{-3} [m]
I_0:	Bias current	0.4 [A]
l_{fu}:	Distance from COG	4.99×10^{-2} [m]
l_{fl}:	to AMB	1.676×10^{-1} [m]
l_{f1}:	Distance from COG	25.35×10^{-3} [m]
l_{f2}:	to sensor	188.15×10^{-3} [m]
g_s:	sensor gain	80000 [V/m]

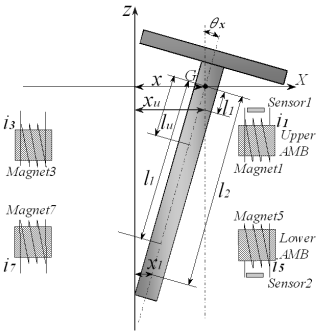

FIGURE 2: Schematic diagram of X-Z plane

Defining the state variables $x = [x\ \theta\ \dot{x}\ \dot{\theta}]^T$, the control inputs $u = [f_u\ f_l]^T$, and the measurment outputs $y = [y_u\ y_l]^T$, we have the state-space equation from Eq.(1), Eq.(2), and Eq.(3) as follows:

$$\begin{aligned} \dot{x} &= A_f x + B_f u, \\ y &= C_f x, \end{aligned} \tag{4}$$

where

$$A_f = \begin{bmatrix} 0 & 0 & 1 & 0 \\ 0 & 0 & 0 & 1 \\ 0 & 0 & 0 & 0 \\ 0 & 0 & 0 & 0 \end{bmatrix},\ B_f = \begin{bmatrix} 0 & 0 \\ 0 & 0 \\ \dfrac{1}{M} & \dfrac{1}{M} \\ -\dfrac{l_u}{I_r} & -\dfrac{l_l}{I_r} \end{bmatrix},$$

$$C_f = g_s \times \begin{bmatrix} 1 & -l_1 & 0 & 0 \\ 1 & -l_2 & 0 & 0 \end{bmatrix}.$$

The equation of motion for Y-Z plane are the same as X-Z plane.

H_∞ CONTROLLER DESIGN

In our approach, an H_∞ controller is designed so that the control inputs are regarded as the attraction forces generated by AMBs. Then, the control currents which generate the desired attraction forces are calculated back based on the nonlinear equation.

The H_∞ controller is designed to have robustness to disturbances and plant uncertainties. Fig. 3 shows

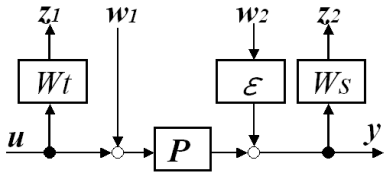

FIGURE 3: Generalized plant

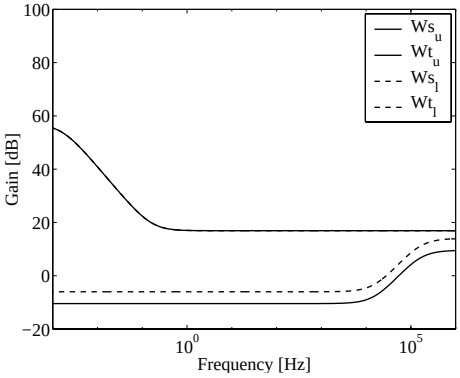

FIGURE 4: Weighting functions

the generalized plant which is used for designing H_∞ controller. W_s is a weighting function for disturbance attenuation, and it is selected to have a large gain at low frequency. On the other hand, W_t is a weight for robust stability, and it is selected to have a large gain at high frequency. The AMB system has two-input and two-output, and these weighting functions are selected as diagonal transfer matrix as follows:

$$W_s = \begin{bmatrix} W_{su} & O \\ O & W_{sl} \end{bmatrix}, \quad W_t = \begin{bmatrix} W_{tu} & O \\ O & W_{tl} \end{bmatrix}$$

In this AMB system, the flywheel is attached on the rotor, and the center of gravity is located above the upper AMB. Thus, the balance of the weighting functions for the upper and the lower AMBs might be very important. The weighting functions should also be optimized considering the balance of the control input of the upper and the lower AMBs in order to have a good transient response when the rotor levitates from touchdown. After some trial and error, we have the following weighting functions and $\varepsilon = 10^{-4}$:

$$\begin{cases} W_{s_u} = \dfrac{s+1}{s+10^{-2}} \times 7 \\ W_{s_l} = \dfrac{s+1}{s+10^{-2}} \times 7 \end{cases} \quad \begin{cases} W_{t_u} = \dfrac{s+1\times10^5}{s+1\times10^6} \times 3 \\ W_{t_l} = \dfrac{s+1\times10^5}{s+1\times10^6} \times 5 \end{cases} \tag{5}$$

The frequency responses of these weights are shown in Fig. 4. Using these weights and the generalized plant of Fig. 3, the H_∞ controller was calculated using MATLAB. The minimum H_∞ norm is $\gamma = 0.51$ and the frequency response of the H_∞ controller is shown in Fig. 5.

SWITCHING ALGORITHMS OF AMBS

In the previous section, we could obtain the H_∞ controller. However it was assumed that the control inputs

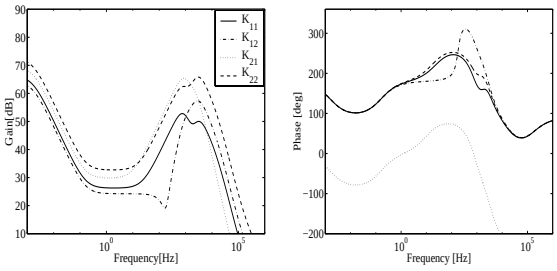

(a) Gain (b) Phase

FIGURE 5: Bode plot of H_∞ controller

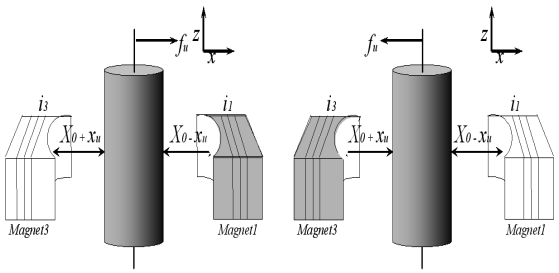

(a) In case of $f_u > 0$ (b) In case of $f_u < 0$

FIGURE 6: Upper AMB

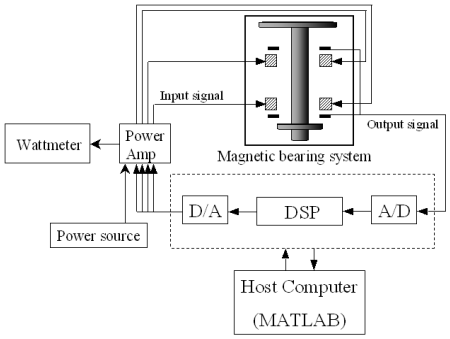

FIGURE 7: Experimental system

are attraction forces generated by AMBs. Thus, the electromagnetic forces should be converted to the control currents in order to implement the controller to the experimental system. In our approach, the AMBs of the left and the right side are switched based on the sign of the attraction force and the coil current of the activated AMB is calculated by nonlinear equations in real-time to generate the forces corresponded to the output of the H_∞ controller. For simplicity, we assume that the inductance of AMB can be neglected because a current feedback amplifier is used in our experimental system. The upper side and the lower side can be considered independently, therefore, the switching condition of the upper side is only shown.

i) In case of $f_u > 0$

When f_u has a positive sign, the magnet 1 must generate the attractive force as shown in Fig. 6(a). Since the relation between f_u and the coil current i_1 are governed by the equation

$$f_u = k_u \frac{i_1^2}{(X_0 - x_u)^2},$$

the coil currents of the upper AMBs can be obtained as

$$i_1 = (X_0 - x_u)\sqrt{\frac{f_u}{k_u}}, \quad \text{and} \quad i_3 = 0.$$

ii) In case of $f_u < 0$

When f_u has a negative sign, the magnet 2 must generate the attractive force as shown in Fig. 6(b). Solving the equation

$$-f_u = k_u \frac{i_3^2}{(X_0 + x_u)^2}$$

with respect to i_3, we have

$$i_1 = 0, \quad \text{and} \quad i_3 = (X_0 + x_u)\sqrt{\frac{-f_u}{k_u}}.$$

EXPERIMENT

Levitation experiment Fig. 7 shows the experimental setup. The displacements at the upper and the lower AMB are measured by eddy-current sensors, and they are fed into DSP through a 4ch 16bit A/D converter. The command signals corresponding to the electric current of AMBs are fed into power amplifier through a 8ch DA converter. The amplifier has an electric current feedback scheme, and the effect of the inductance of AMB can be neglected whenever the amplifier is not saturated. The control algorithm is implemented by C language, and it is executed on digital signal processor (DSP) TMS320C6701. We can access and monitor any variables on DSP program via MATLAB. The sampling frequency is 20kHz and the obtained H_∞ controller is discretized by Tustin transformation for the discrete-time implementation.

Firstly, we carried out the levitation experiment. Fig. 8 shows the orbits of the rotor at the upper and the lower side, and it can be confirmed that they are controlled at the origin of X-Y axis precisely. The electric currents of AMBs are shown in Fig. 9. We can confirm that the currents at the upper side are switched correctly. However, at the lower side, the currents of i_7 and i_5 are not switched evenly, and we consider that this phenomenon caused by the interference from the axial AMB which is controlled by the PID controller.

Rotation experiment In the previous section, we confirmed that the proposed method can levitate the rotor without bias currents. Thus, in this section, we curried out rotation experiments up to 100Hz corresponding to 6000rpm. Fig. 10 shows the orbits of the rotor at ω=100 Hz, and the electric currents of AMBs are also shown in Fig. 11. From these figures, it is confirmed that the rotor is controlled around the origin of X-Y axis without destabilizing the system. The orbit of the rotor at the lower side is larger than that at the upper side,

TABLE 2: Rotational frequency vs Power consumption

	Rotational frequency (Hz)			
	0	10	20	30
Zero-bias method (W)	64.8	64.4	64.4	70.9
Bias method (W)	112.2	111.7	112.1	112.1
Energy reduction (%)	48 %	47 %	48 %	41 %

and it can be consider that the distance from the centre of gravity to the lower AMB is longer than that at the upper side. The electric currents of all the AMBs have half-wave form, and it is switched correctly. Moreover, it is confirmed that the control currents include high frequency components because the gain of the controller is relatively high at high frequency. We tried to increase the rotation speed over 100Hz, however, we could not succeed it. Before the system becomes unstable, we observed a distinctive orbit induced by gyro-effect.

Comparison to a conventional method The performance of the proposed method is compared with that obtained by a conventional method using bias current by experiments. The linearized model of the plant was obtained assuming the bias current of 0.5[A], and the H_∞ controller was calculated. The control performances are evaluated in terms of step response, impulse response, and levitation and rotation performance. We note that a step reference and an impulse disturbance are imposed at upper AMB only.

The experimental results of a levitation test are shown in Fig. 12 and Fig. 13. The orbit is very small, and it is difficult to find the difference between Fig. 8 and Fig. 12. Thus, we magnify X and Y axis as shown in Fig. 14 and Fig. 15. From these figures, the orbit of the conventional method is a little bit smaller than that of the proposed method, and it can be considered that the discontinuous action of the proposed method degrades the control accuracy. Fig. 16 and Fig. 17 show the step response, and the proposed method achieves a fast settling time and a small overshoot compared with the conventional method. In the conventional method, it was difficult to increase the gain of the controller to have a fast response because the control input is defined as the fluctuation from the bias current and it can not exceed the bias current. Actually, from Fig. 17(a) and Fig. 17(d), it can be observed the control input of the conventional method is saturated around $t = 0$.

Comparison of the power consumption We evaluate the power consumption of the proposed method and the conventional method in levitation and rotation experiments. The power consumption of the control box which has an electric current amplifier is measured by a digital power meter as shown in Fig. 7. Table 2 shows the results for each rotational frequency of ω=0 Hz, 10 Hz, 20 Hz, and 30 Hz. The result at 0 Hz shows the power consumption required to levitate the rotor without rotation. As shown in Table 2, the power consumption of the proposed method for each rotation speed is lower than that of the bias method, and the average reduction rate is 46 percent. We note that the conventional method can not stabilize the system more than 30Hz. The orbits of

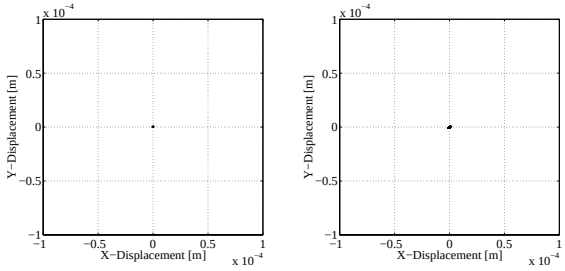

(a) Upper side (b) Lower side

FIGURE 8: Orbits of rotor at ω=0 Hz

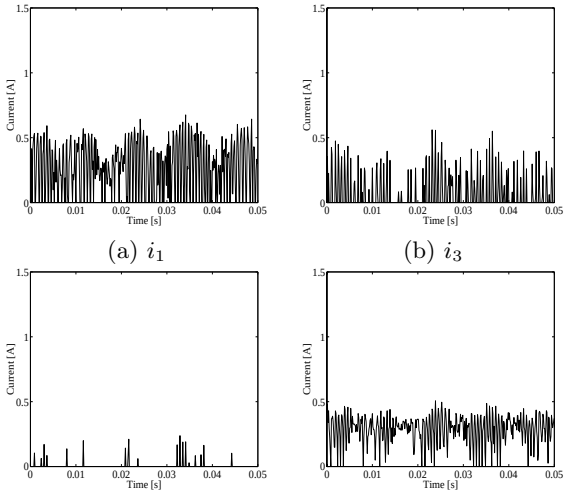

(a) i_1 (b) i_3

(c) i_5 (d) i_7

FIGURE 9: Control currents at ω=0 Hz

the rotor of the proposed method and the conventional method at 30Hz are shown in Fig. 18, Fig. 19, Fig. 20 and Fig. 21.

CONCLUSION

In this study, we have proposed a simple and effective method which does not use bias current based on H_∞ control with simple linearization. The H_∞ controller has been designed based on the mathematical model of the plant, where the electromagnetic force is regarded as control input, and then the coil currents have been calculated back by nonlinear equation in real-time to generate the forces correspond to the output of the H_∞ controller. The effectiveness of the proposed method has been evaluated by simulation and experiment.

If the rotation speed can be increased more, we might expect to reduce the power consumption less than that required to levitate the rotor because the self-stability of the rotor is increased at high speed rotation. As a future work, we will work toward to achieve zero power control by utilizing the self-stability of the rotor and the zero bias control.

REFERENCES

[1] R.Gasch, H.Pfützner: Rotordynamik Eine Einführung, Springer-Verlag, 1975.

[2] S.Sivrioglu, and K.Nonami: Adaptive Output Backstepping Control of a Flywheel Zero-Bias AMB System with Parameter Uncertainty, Proc. of the 42nd IEEE Conference on Decision and Control, pp.3942–3947, 2003

[3] Y.Ariga, K.Nonami, and K.Sakai: Nonlinear Control of Zero Power Magnetic Bearing Using Lyapnov's Direct Method, Proc. of the 7th International Symposium on Magnetic Bearing, pp.293–298, 2000.

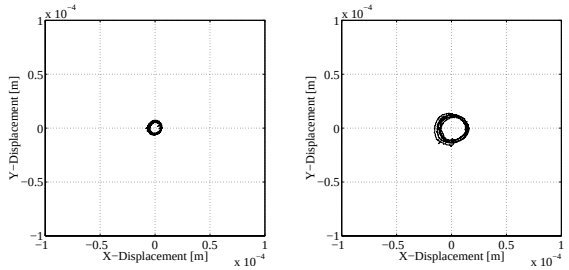

(a) Upper side (b) Lower side

FIGURE 10: Orbits of rotor at ω=100 Hz

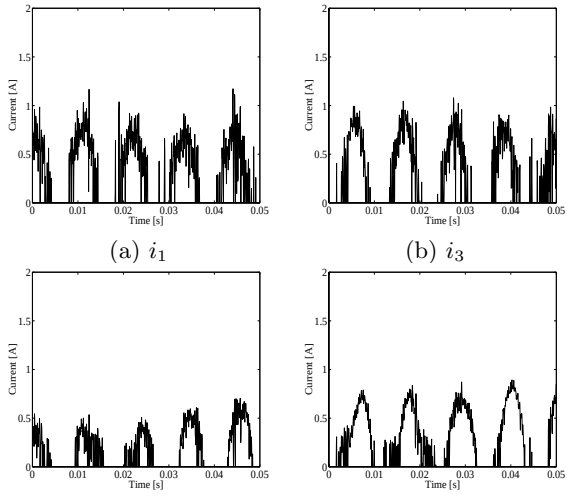

(a) i_1 (b) i_3

(c) i_5 (d) i_7

FIGURE 11: Control currents at ω=100 Hz

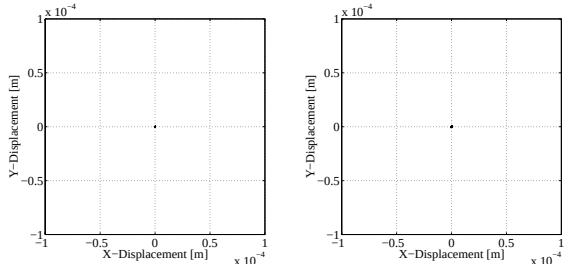

(a) Upper side (b) Lower side

FIGURE 12: Orbits of rotor at ω=0Hz by the bias method

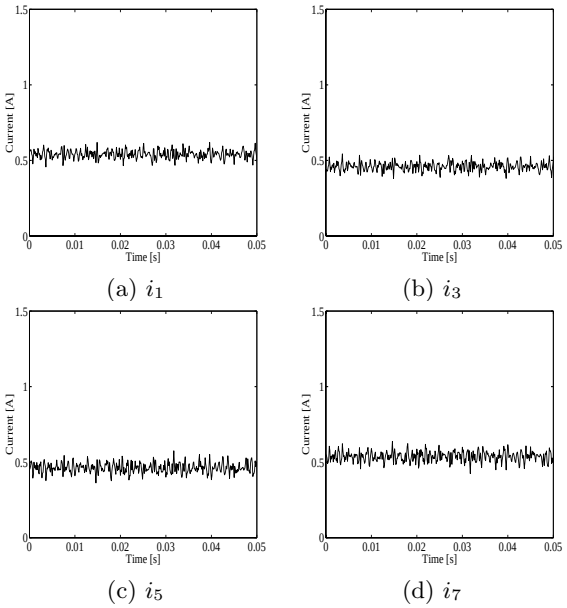

(a) i_1 (b) i_3

(c) i_5 (d) i_7

FIGURE 13: Control currents at ω=0Hz by the bias method

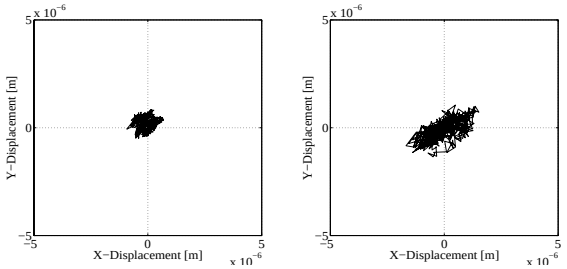

(a) Upper side (b) Lower side

FIGURE 14: Orbits of rotor at ω=0Hz by the proposed method (Magnified)

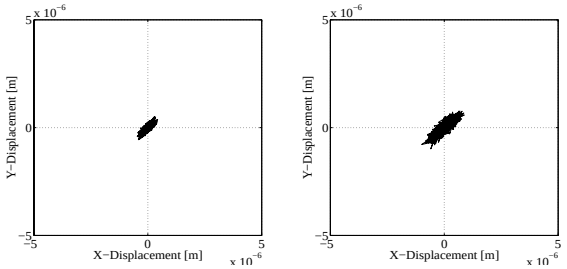

(a) Upper side (b) Lower side

FIGURE 15: Orbits of rotor at ω=0Hz by the bias method (Magnified)

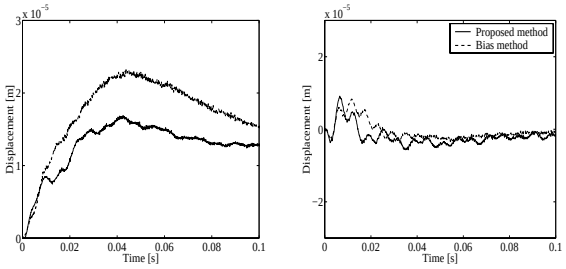

(a) Upper side (b) Lower side

FIGURE 16: Step response

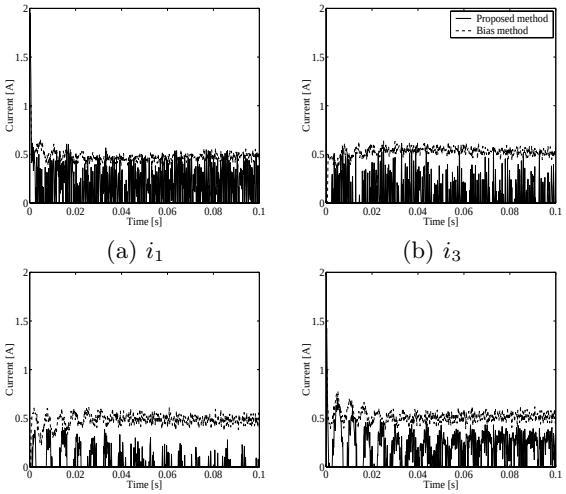

(a) i_1 (b) i_3

(c) i_5 (d) i_7

FIGURE 17: Control currents of step response

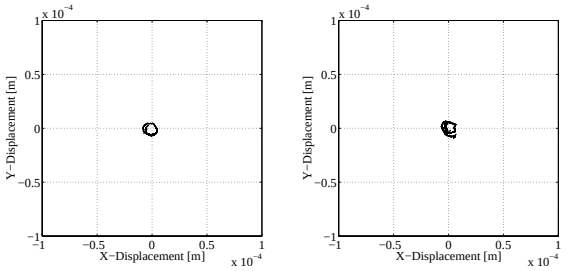

(a) Upper side (b) Lower side

FIGURE 18: Orbits of rotor at ω=30Hz by the proposed method

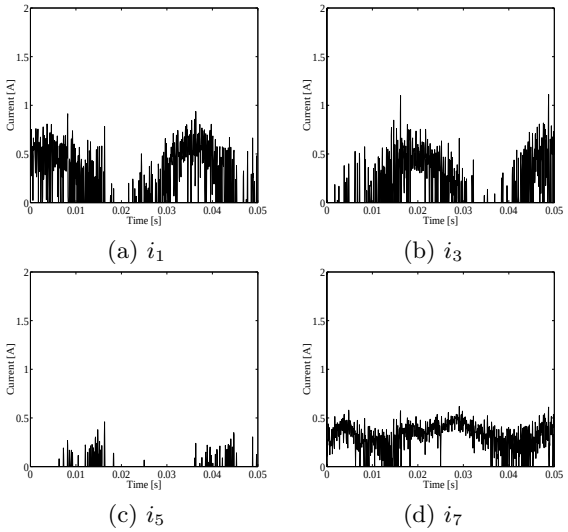

(a) i_1 (b) i_3

(c) i_5 (d) i_7

FIGURE 19: Control currents at ω=30Hz by the proposed method

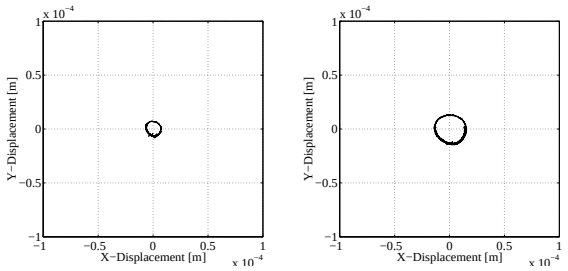

(a) Upper side (b) Lower side

FIGURE 20: Orbits of rotor at ω=30Hz by the bias method

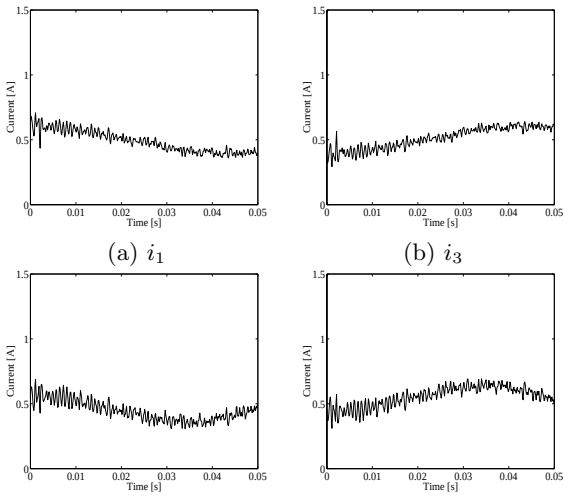

(a) i_1 (b) i_3

(c) i_5 (d) i_7

FIGURE 21: Control currents at ω=30Hz by the bias method